

Article

Open Access

J. Mex. Chem. Soc. **2026**, 70(1):e2105

Received November 1st, 2022
Accepted May 11th, 2023

<http://dx.doi.org/10.29356/jmcs.v70i1.2105>
e-location ID: 2105

Keywords:

TRPV1 antagonist, 3D-QSAR, molecular docking, ADMET prediction, BCTC derivatives

Palabras clave:

Antagonista de TRPV1, 3D-QSAR, acoplamiento molecular, predicción ADMET, derivados del BCTC

*Corresponding author:

Toughzaoui Abdelilah
email:
abdelilah.toughzaoui@usmba.ac.ma

©2026, edited and distributed by Sociedad
Química de México

ISSN-e 2594-0317

In silico Studies of *N*-(4-tert-butylphenyl)-4-(3-chloropyridin-2-yl) piperazine-1-carboxamide Derivatives as Potent TRPV1 Antagonists using 3D QSAR, ADMET and Molecular Docking

Toughzaoui Abdelilah^{1*}, Chedadi Oussama², El Aissouq Abdellah², El Ouardi Youssef³, Bouachrine Mohammed⁴, Ouammou Abdelkrim¹, Moradi Kamal¹

¹LIMOME Laboratory, Faculty of Sciences Dhar El Mahraz, Sidi Mohamed Ben Abdellah University, Fez, Morocco.

²Laboratory of Processes, Materials and Environment (LPME), Faculty of Science and Technology, Sidi Mohamed Ben Abdellah University, Fez, Morocco.

³Laboratory of Separation Technology, Lappeenranta University of Technology, Lappeenranta, Finland.

⁴MCNS Laboratory, Faculty of Sciences, Moulay Ismail University, Meknes, Morocco.

Abstract. TRPV1 is a promising therapeutic target given its involvement in pain management and inflammation. TRPV1 antagonists are increasingly sought after for their analgesic, anti-inflammatory and antitumor properties with fewer side effects. This study focused on the design of new effective TRPV1 antagonists by replacing the pyridine ring of BCTC with a pyrimidine ring. Significant 3D-QSAR models were developed using CoMSIA and CoMFA methods and showed a satisfactory correlation between experimental and predicted activity ($Q^2 = 0.715$; $R^2 = 0.988$; $SEE = 0.048$). Electrostatic, hydrophobic fields and hydrogen bond acceptors contributed significantly to the biological activity of studied compounds as well as the importance of hydrophobic, electrostatic fields and H-bond acceptors on the antagonistic activity of the most active molecule in the series of compounds studied. Molecular docking analysis validated the 3D-QSAR models and explained the interactions of the most active ligands with the binding site. These results permitted the prediction of new compounds, whose pharmacokinetic properties, toxicity and pharmacodynamics effects were assessed using ADMET and drug similarity.

©2026, Sociedad Química de México. Authors published within this journal retain copyright and grant the journal right of first publication with the work simultaneously licensed under a [Creative Commons Attribution License](#) that enables reusers to distribute, remix, adapt, and build upon the material in any medium or format for noncommercial purposes only, and only so long as attribution is given to the creator.



Resumen. El TRPV1 es un objetivo terapéutico prometedor debido a su participación en el manejo del dolor y la inflamación. Los antagonistas del trpv1 son cada vez más buscados por sus propiedades analgésicas, antiinflamatorias y antitumorales con menos efectos secundarios. Este estudio se centró en el diseño de nuevos antagonistas efectivos del trpv1 mediante la sustitución del anillo de piridina del bctc por un anillo de pirimidina. Se desarrollaron modelos 3D-QSAR significativos utilizando los métodos Comsia y Comfa, que mostraron una correlación satisfactoria entre la actividad experimental y la prevista ($Q^2 = 0.715$; $R^2 = 0.988$; $SEE = 0.048$). Los campos electrostáticos e hidrofóbicos y los aceptores de enlaces de hidrógeno contribuyeron significativamente a la actividad biológica de los compuestos estudiados. El análisis de acoplamiento molecular validó los modelos 3D-QSAR y explicó las interacciones de los ligandos más activos con el sitio de unión. Estos resultados permitieron predecir nuevos compuestos, cuyas propiedades farmacocinéticas, toxicidad y efectos farmacodinámicos se evaluaron mediante ADMET y por similitud con fármacos.

Introduction

Chronic pain has been considered to be pain that lasts beyond the normal healing time [1] and hence lacks the acute warning function of physiological nociception[2]. TRPV1(transient receptor potential vanilloid type 1) is among the various targets involved in pain transmission, it is a non-selective polymodal calcium ion channel [3]expressed on sensory neurons [4]. by translating and integrating stimuli through the transmission of calcium-based signals. TRPV1 serves as a link between the cellular response ,and the extracellular environment [5]. TRPV1 is activated by natural vanilloids such as capsaicin[6,7], resiniferatoxin, heat ($T > 43^\circ$) [8], acid ($pH= 6; 8$) [9],or endogenous stimuli like anandamide, linoleic acid and proinflammatory cytokines [10]. TRPV1 antagonists are also viewed as interesting analgesics [4]. Although several potent TRPV1 antagonists have been developed to date [11], their use has been limited due to adverse side effects such as hyperthermia and analgesia [12]. While there are no antagonists that haven't been clinically tested yet, urea piperazines, particularly BCTC, are considered one of the leading classes of TRPV1 antagonists. However, BCTC has shown negative effects on TRPV1 activation [13]by capsaicin and protons but resulting in hyperthermia. Over the past decade, many research efforts have been devoted to the optimisation of the BCTC-based molecule, leading to the development of several series of analogues. Structural analyses showed that substitution of the pyridine group with pyrimidine moieties [14] improved the interaction with TRPV1 receptors and provided greater versatility in synthesis due to its lower p-electron density which impacts chemical reactivity [15].

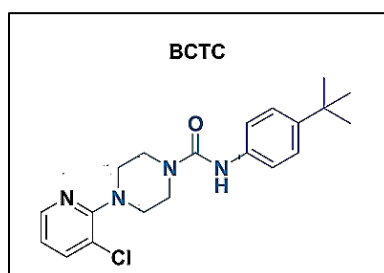


Fig. 1. BCTC chemical structure.

Computer-aided drug design uses computational approaches such as 3D QSAR to reduce the expense and time associated with the drug discovery process [16]. The bioisosteric property of pyridine in BCTC has provided the opportunity to improve the interaction with the TRPV1 receptor.

Modern pharmaceutical chemistry has enabled the pharmaceutical industry to develop efficient and selective searches using techniques such as molecular docking [17]. This technique is used to find the optimal conformation of a ligand in its receptor by generating all the conformations of the receptor complex and ranking

them according to their binding energy stability. The pharmacokinetic properties of the predicted compounds were analyzed by predicting drugs similarity and the ADMET method [18].

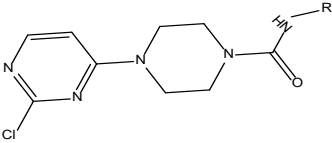
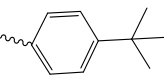
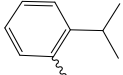
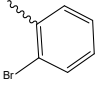
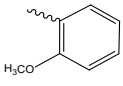
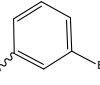
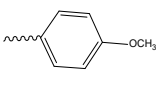
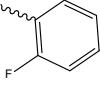
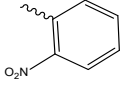
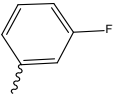
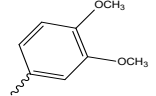
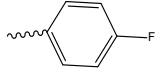
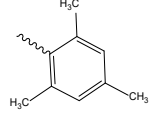
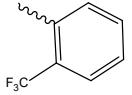
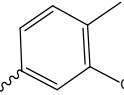
In this study, the 3D quantitative structure activity relationship (QSAR), molecular docking, ADMET (absorption, distribution, metabolism, excretion and toxicity) were applied to a new series of *N*-(4-tert-butylphenyl)-4-(3-chloropyridin-2-yl) piperazine-1-carboxamide as TRPV1 antagonists [19]. The overall objective is to predict new TRPV1 antagonists with high activity than the most active compound in this series.

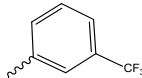
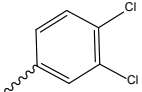
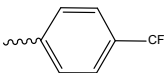
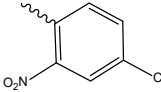
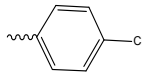
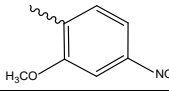
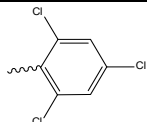
Experimental

Biological database

The biological database chosen for this study included 21 derivatives compounds of *N*-(4-tert-butylphenyl)-4-(3-chloropyridin-2-yl)piperazine-1-carboxamide extracted from the published literature and associated with their biological activity (IC_{50}) [20]. The IC_{50} values express the concentration required to inhibit 50% of the TRPV1 antagonist activity, were expressed as pIC_{50} following the relation: $pIC_{50} = -\log (IC_{50} \cdot 10^{-6})$. The database was divided into two groups: the training set with 16 molecules and the test set with 5 molecules. All compounds were designed and optimized using ChemOffice 3D and SYBYL.X- 2.0 [21] software. The chemical structures and corresponding biological data are presented in Table 1.

Table. 1. Dataset of 2*N*-(4-tert-butylphenyl)-4-(3-chloropyridin-2-yl) piperazine-1-carboxamide derivatives with their corresponding experimental activity.

					
Compounds		pIC_{50}	Compounds		pIC_{50}
M01		4,537	M11 ^T		5,123
M02		5,969	M12 ^T		5,026
M03		5,838	M13		4,387
M04		6,104	M14		6,068
M05		6,021	M15		4,431
M06 ^T		5,942	M16		4,455
M07 ^M		6,866	M17 ^T		4,346

Compounds		pIC50	Compounds		pIC50
M08		6,265	M18		4,267
M09 ^T		6,058	M19		4,366
M10 ^T		5,903	M20		4,376
			M21		4,167

^T Indicates the compounds of the test set for 3D-QSAR models.

3D-QSAR

Molecular alignment

SYBYL.X-2.0 software [21] was used to perform the calculations and optimize the structures. The geometries of all molecules were optimised using the conjugate gradient method with a convergence factor of 0.001 kcal/mol Å and 5000 iterations, using the Tripos force field [22]. Atomic partial charges of the Gasteiger-Hückel type [16,26] were used. To align the database, the "Distil Rigid" option was used, choosing the compound M07 as a template. Each analogue was aligned to the model by minimizing the RMSD value through rotation and translation. The results of the alignment procedure are shown in Fig. 2.

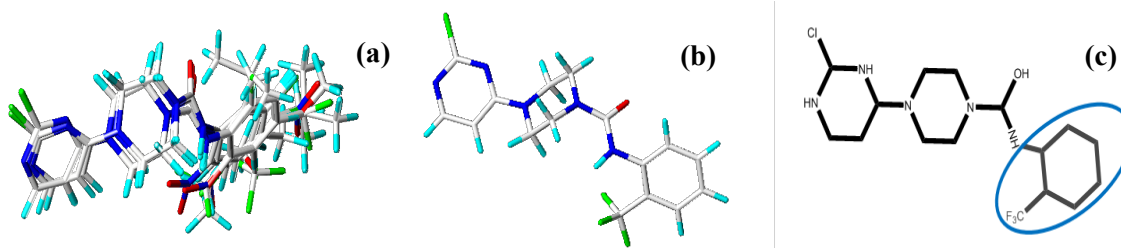


Fig. 2. Molecular alignment of compounds: **(a)** Alignment of training set compounds. **(b)** Molecular common core, and **(c)** M07: most active compound in data base.

Analytic study of CoMFA and CoMSIA

Comparative Molecular Field Analysis (CoMFA) [23] is a method used to model the biological activity of a molecule, which generally depends on its interaction with a given receptor [22]. The modeling of this activity can therefore be carried out by calculating the interactions of each molecule (ligand) with this receptor, and by establishing a relationship between these interactions and the activity studied [24]. The modelling of this activity can therefore be carried out by calculating the interactions of each molecule (ligand) with this receptor [25], and by establishing a relationship between these interactions and the activity studied. The energy calculation is done by putting an appropriate probe on the ligand at each grid point. The electrostatic (Coulombian) and steric (van der Waals) [26] properties are evaluated at each unit fraction and the results

obtained are used as descriptors [27] to develop 3D QSAR model. The values of these descriptors are then related to biological responses using robust linear regression method such as partial least squares (PLS) [28].

Comparative Molecular Similarity Index Analysis (CoMSIA)

The CoMSIA method includes 5 distinct similarity fields [29]. These are the steric, electrostatic, hydrophobic, hydrogen bond donor and hydrogen bond acceptor fields. These fields cover the major types of interaction involved in ligand receptor binding. This is an extension of CoMFA such that the similarity indices are calculated in 3D matrix comparable to CoMFA. The distance-dependent potentials between the probe and the molecule are modeled by Gaussian [30] function. The form of this function is different from that of classical potential functions and allows the calculation of similarity indices for all points in the matrix, both inside and outside the Van der Waals surface [26].

PLS analysis

In order to develop a powerful QSAR model, the electrostatic and steric energies of each ligand at each grid point are calculated using appropriate probes. The calculated values are then used as descriptors for the model. A robust linear regression method, such as partial least squares (PLS) [28], is used to correlate these descriptors with the biological responses. The filtering of the columns was performed with energy threshold of 30 kcal/mol, with a default value of 2.0 kcal/mol in the cross-validation. The leave-one-out cross-validation method is used to determine the correlation coefficient Q^2 and the optimal number of components (ONC).

$$Q^2 = 1 - \left(\frac{\sum_{i=1}^{training} (Y_{iobs} - Y_{ipred})^2}{\sum_{i=1}^{training} (Y_{iobs} - \bar{Y})^2} \right)$$

Where Y_{ipred} and Y_{iobs} are the observed predicted and observed values of activity. \bar{Y} is average value of activity of the training set.

The best performing 3D QSAR model is selected using Q^2 and R^2 values, with criteria of $Q^2 > 0.5$ and $R^2 > 0.6$ and low standard error of estimation. In addition, external validation is performed on a test set of five molecules using the R^2 test value, which must be greater than 0.6 to judge the predictive ability of the resulting QSAR model.

$$R^2_{test} = 1 - \left(\frac{\sum_{i=1}^{test} (Y_{iobs(test)} - Y_{ipred(test)})^2}{\sum_{i=1}^{training} (Y_{iobs(test)} - \bar{Y}_{itraining})^2} \right)$$

Where Y_{ipred} and Y_{iobs} are the observed predicted and observed values of activity the test set compounds and $\bar{Y}_{itraining}$ indicates mean activity value of the training set.

Molecular docking

In molecular modelling, molecular docking [31,32] is a method that calculates and searches the preferred orientation of molecule (*ligand derived from N-(4-tert-butylphenyl)-4-(3-chloropyridin-2-yl) piperazine-1-carboxamide*) to receptor (*proteins (PDB code: 5IS0)*) when bound to form stable complex. The parameters of docking calculation [33] are: preparation ligand (position, orientation and random or precise conformation), the grid box size used (rectangular parallelepiped) grid box with coordinates ($x=125.93$, $y=139.947$, $z=100.841$ to 0.375) with number of points ($x=24$, $y=42$, $z=44$) centred on the active site of the protein, and finally, registration of the best interaction between the ligand and receptor. When molecular docking parameters have been set, the ligand can be docked to the receptor. After the parameters of the molecular docking are established, the program moved to the prediction and evaluation stage. The visualization of potential interaction modes was done using Discovery Studio 2017 software [34]. The redocking approach was used to validate the docking method by redocking the co-crystallised ligand and calculating the RMSD between the reference and the redocked co-crystals. The best superposition obtained is shown in Fig. 3. The RMSD value is 1.587 Å, indicating that the approach accurately predicted the binding affinity of the ligand.

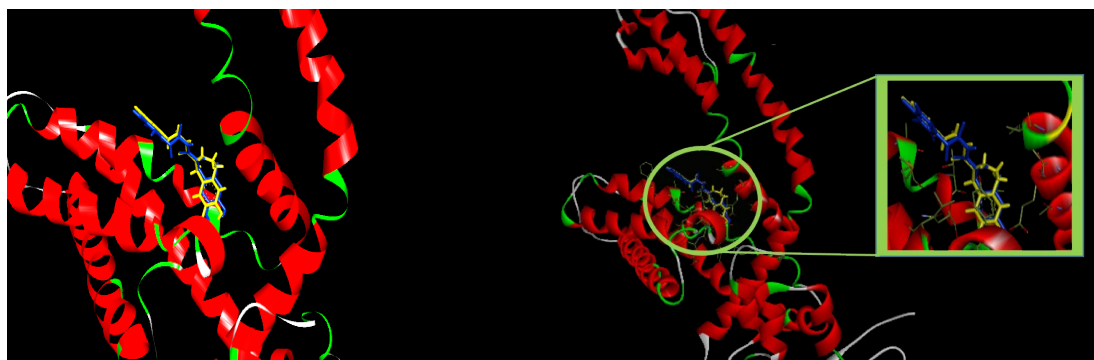


Fig. 3. the Superposition of the reference ligand on protein pocket. The blue stick represents the redocked ligand, and the yellow stick represents the reference ligand.

Results and discussion

Statistical analysis of the 3D-QSAR model

The statistical results of CoMFA and CoMSIA models are presented in Table 2.

Table 2. Statistical analysis of CoMFA and CoMSIA models using PLS method.

	CoMFA	CoMSIA
$Q^2 = R^2_{cv}$	0.686	0.715
R^2	0.981	0.988
ONC	5	4
SEE	0.115	0.048
R^2_{test}	0.703	0.874
F value	238.4	701.74
Steric	0.502	-
Electrostatic	0.498	0.535
Hydrophobic	-	0.303
H-B Donor	-	-
H-B Acceptor	-	0.162

Q^2 : Cross-validated correlation coefficient

R^2 : Non-cross-validated correlation coefficient;

ONC: Optimum number of components

SEE: Standard error of the estimate;

R^2_{test} : External validation correlation coefficient;

F: F-test value.

The statistical results of the CoMFA model were examined using partial least squares (PLS) regression. The cross- validation correlation coefficient ($Q^2=0.686>0.5$) was obtained with five optimal components, indicating that the model is reliable in predicting pIC_{50} values. The invalidated PLS analysis showed high correlation coefficient ($R^2=0.981$), low standard error estimate ($SEE=0.115$), and F value ($F=238.4$). The electrostatic field and steric field contribution were 49.8% and 50.2%, respectively. The experimental and predicted pIC_{50} values of compounds were presented in the table 3, including residual values for training and test set.

Table 3. experimental, predicted activity and residual values obtained by CoMSIA and CoMFA models.

Compounds	pIC_{50}	CoMFA	Residual	CoMSIA	Residual
M01	4.537	4.571	-0.034	4.541	-0.004
M02	5.969	6.007	-0.038	6.022	-0.053
M03	5.838	5.765	0.073	5.765	0.073
M04	6.104	6.166	-0.062	6.105	-0.001
M05	6.021	5.862	0.159	6.011	0.01
M06 ^T	5.942	6.334	-0.392	5.679	0.263
M07 ^M	6.866	6.839	0.027	6.856	0.01
M08	6.265	6.148	0.117	6.288	-0.023
M09 ^T	6.058	5.811	0.247	6.536	-0.478
M10 ^T	5.903	5.342	0.561	5.791	0.112
M11 ^T	5.123	5.502	-0.379	5.047	0.076
M12 ^T	5.026	5.111	-0.085	5.277	-0.251
M13	4.387	4.446	-0.059	4.351	0.036
M14	6.068	6.12	-0.052	6.073	-0.005
M15	4.431	4.433	-0.002	4.459	-0.028
M16	4.455	4.392	0.063	4.461	-0.006
M17 ^T	4.346	4.501	-0.155	4.258	0.088
M18	4.267	4.466	-0.199	4.313	-0.046
M19	4.366	4.291	0.075	4.356	0.01
M20	4.376	4.258	0.118	4.377	-0.001
M21	4.167	4.162	0.005	4.147	0.02

^T represents the test set compounds.

Fig. 4 shows the graph representing the values predicted by the CoMFA model as a function of the experimental pIC₅₀ values. Most of the points are on the diagonal line of the graph.

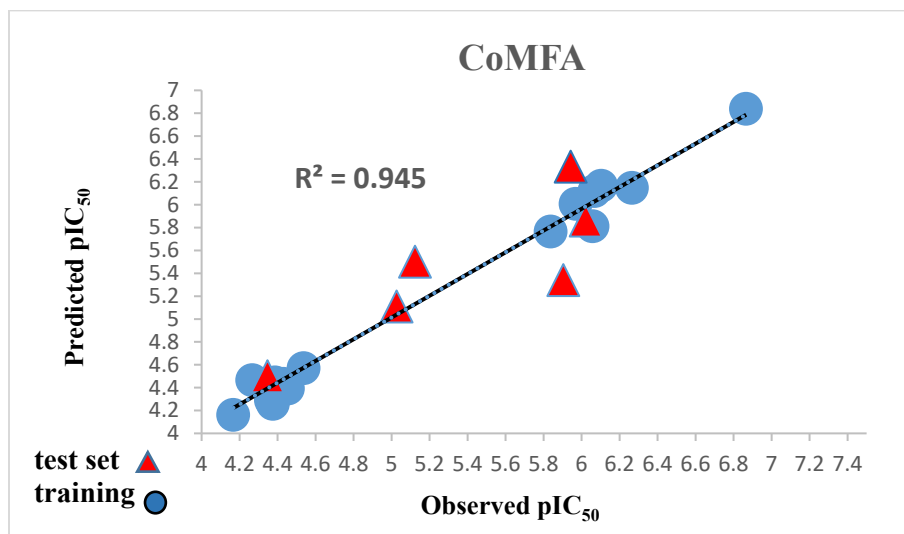


Fig. 4. Correlation graph of predicted activities versus experimental activities (CoMFA).

The utilization of the CoMSIA model resulted in improved statistical parameters. The electrostatic, Hydrophobic, and hydrogen bond acceptor fields significantly influenced the antagonistic activity of TRPV1. The model yielded Q² coefficient of 0.715 with four optimal components, an R² correlation coefficient of 0.988, a low standard error estimate of 0.048, and an F value of 701.74. The contributions of the electrostatic, hydrophobic, and hydrogen bond acceptor fields were 0.535, 0.303, and 0.162 respectively. The predictive correlation coefficient of the test set had an R²_{test} value of 0.874. The experimental and predicted values of pIC₅₀ were presented in Table 2. The plot of experimental pIC₅₀ activity compared with predicted pIC₅₀ activity is shown in Fig. 5, where most points were on the diagonal.

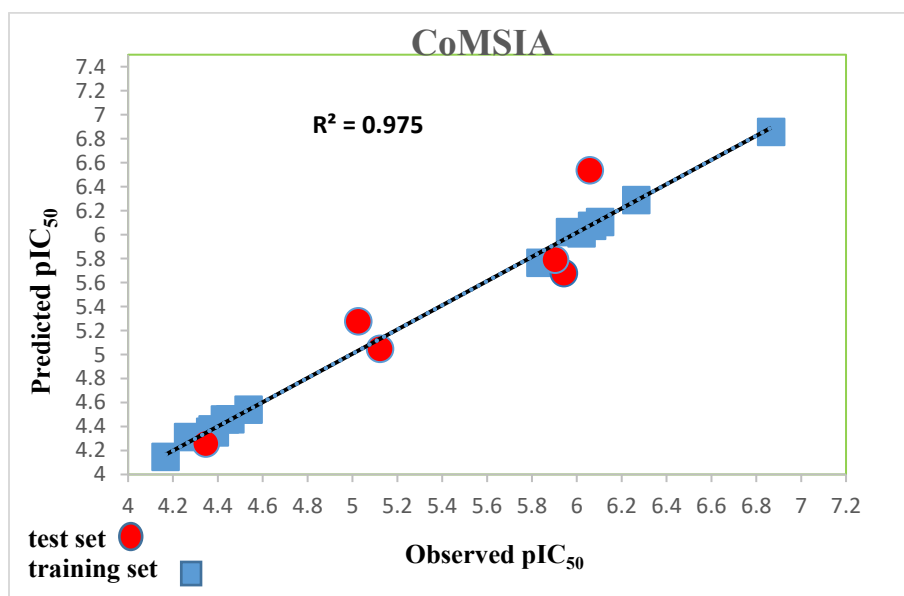


Fig. 5. Correlation graph of predicted activities versus experimental activities (COMSIA).

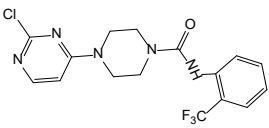
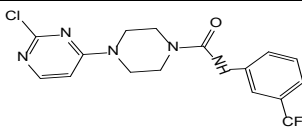
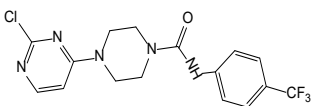
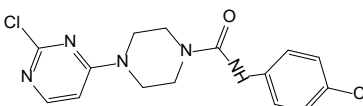
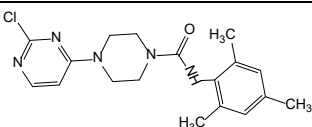
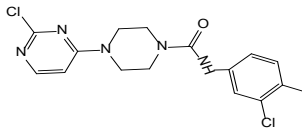
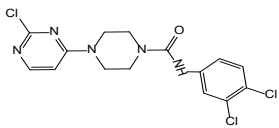
Interpretation of CoMSIA contours

The contour map represented the results of the CoMFA and CoMSIA models and highlighted regions of 3D space where molecular fields predominate. It also helps identify areas where changes in molecular fields are strongly correlated to simultaneous changes with biological activity.

In order to predict new molecules, we rely on the distribution of the molecular fields contributed to our model by targeting on the electrostatic field, which represents about 53 % of the total contribution. and the hydrophobic field, which represents 30 % while the hydrogen bond acceptor field represents 16 % of the total contribution. The contour map relatively specifies the favourable and unfavourable positions for the molecular fields, which helps us construct the SAR.

Fig. 6 shows the molecular field contour map of the CoMFA model for the most active compound M07. The green contours on the map represent the electrostatic field and highlight the regions where the presence of the electron-donor or electro-acceptor group promotes TRPV1 antagonistic activity. It can be seen that the green contour is predominant in the para position of the R substituent. The hydrophobic field, on the other hand, is represented by yellow contours, which indicate regions where the presence of a hydrophobic group in the R-substituent of the substituted benzene enhances activity. While the favourable regions of the hydrogen bond acceptor field are represented by magenta contour, however, the cyan colour indicates unfavourable regions of the presence of the hydrogen bond acceptor field. If we take for example, the most active molecule, M07 ($\text{pIC}_{50}=6.866$). We notice the existence of CF_3 group in ortho position which favours hydrophobic field and the hydrogen bond acceptor which can explain the high activity also of the molecules M08 ($\text{pIC}_{50}=6.265$) and M09 ($\text{pIC}_{50}=6.058$) and we see it clearly in the case of the molecule M10 ($\text{pIC}_{50}=5.903$) with Cl group in para position. If we compare the activity of M16 ($\text{pIC}_{50}=4.455$); M17 ($\text{pIC}_{50}=4.346$); M18 ($\text{pIC}_{50}=4.267$); M19 ($\text{pIC}_{50}=4.366$) with M21 ($\text{pIC}_{50}=4.167$), in which there is the existence of hydrophobic groups in Ortho Meta and para position. In addition, we observe the influence of the existence of groups that favour the electrostatic field in para position. The table 4 lists the structures of the compounds M07 M08 M09 M10 M16 M17 M18 M19 M21 and their biological activities.

Table 4. biological activities and chemical structures.

 <p>M07 ($\text{pIC}_{50}=6.866$)</p>	
 <p>M08 ($\text{pIC}_{50}=6.265$)</p>	 <p>M09 ($\text{pIC}_{50}=6.058$)</p>
 <p>M10 ($\text{pIC}_{50}=5.903$)</p>	 <p>M16 ($\text{pIC}_{50}=4.455$)</p>
 <p>M17 ($\text{pIC}_{50}=4.346$)</p>	 <p>M18 ($\text{pIC}_{50}=4.267$)</p>

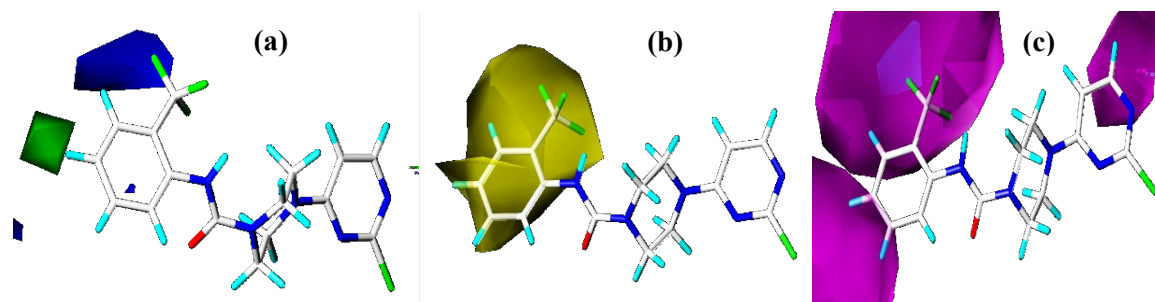
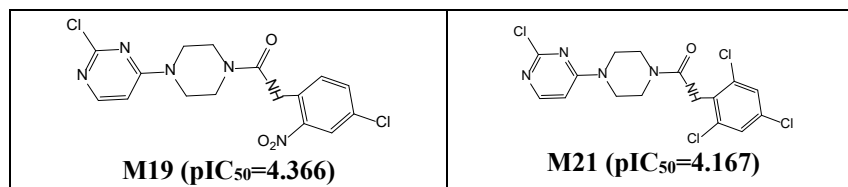


Fig. 6. The contour maps of the CoMSIA analysis of TRPV1 antagonistic activity for compound M07 (a) electrostatic contour maps, (b) hydrophobic contour maps, and (c) contour map showing hydrogen binding of the acceptor.

SAR summarized results

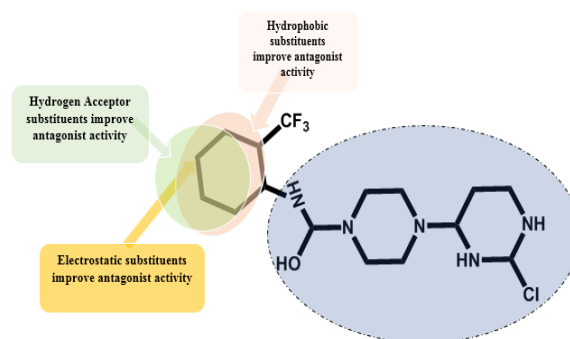


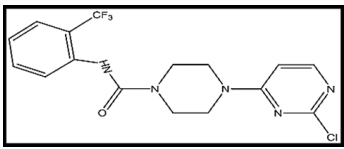
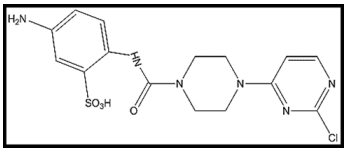
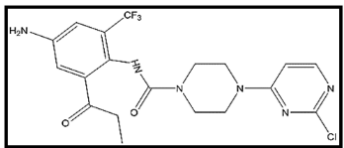
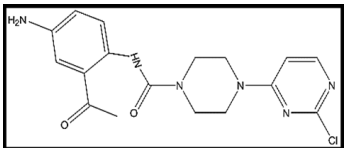
Fig. 7. (SAR: Structure Activity Relationship) information provided by the 3D-QSAR analysis. of molecules M07.

Development of New TRPV1 antagonist

The development and design of new TRPV1 antagonists is based on the results of 3D-QSAR modeling and molecular docking [29] to improve the activity of the predicted compounds. The 3D-QSAR model revealed that electrostatic, hydrophobic fields and hydrogen bond acceptors are crucial in describing and explaining the activity of the investigated compounds. Based on the information obtained from the best selected 3D-QSAR model we proposed a new series of antagonists by modifying some structural characteristics. The chemical structures, their predicted activities and binding affinity score values are listed in Table 5. All predicted compounds have pIC₅₀ values higher than the most potent antagonist in the dataset (compound M07), indicating that our model is reliable and can be used to predict new TRPV1 antagonists.

Molecular docking results

Table 5. activity and binding energy values of M07 and the predicted compounds.

Complex	pIC ₅₀	Binding Energy (kcal mol ⁻¹)	Predicted compounds
M07	6.832	-6.01	
P1	7.168	-6.87	
P2	7.135	-6.28	
P3	6.948	-6.02	

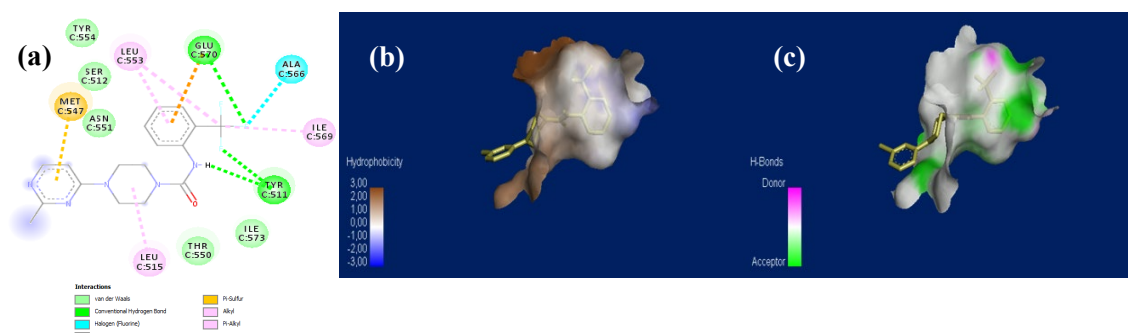


Fig. 8. Interaction of M07 with the protein (PDB ID: 5IS0). **(a)** 2D visualization of the interactions at the binding site; **(b)** hydrophobicity (3D view); and **(c)** 3D representation of the hydrogen bonding conformation

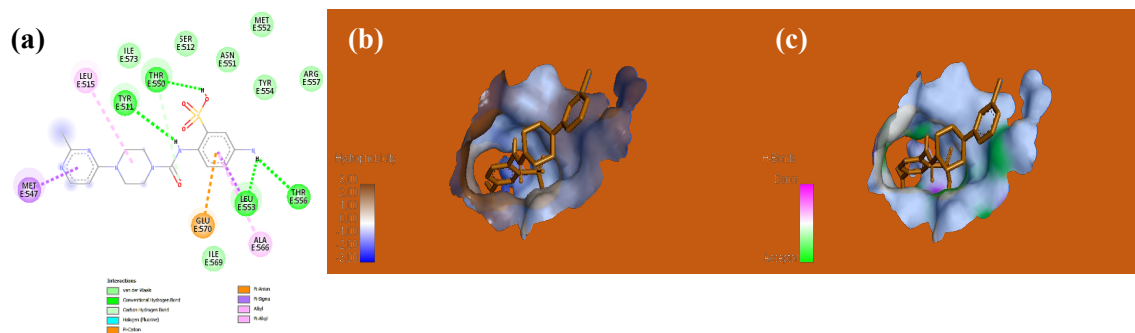


Fig. 9. Interaction of P1 with the protein (PDB ID: 5IS0). **(a)** 2D visualization of the interactions at the binding site; **(b)** hydrophobicity (3D view); and **(c)** 3D representation of the hydrogen bonding conformation.

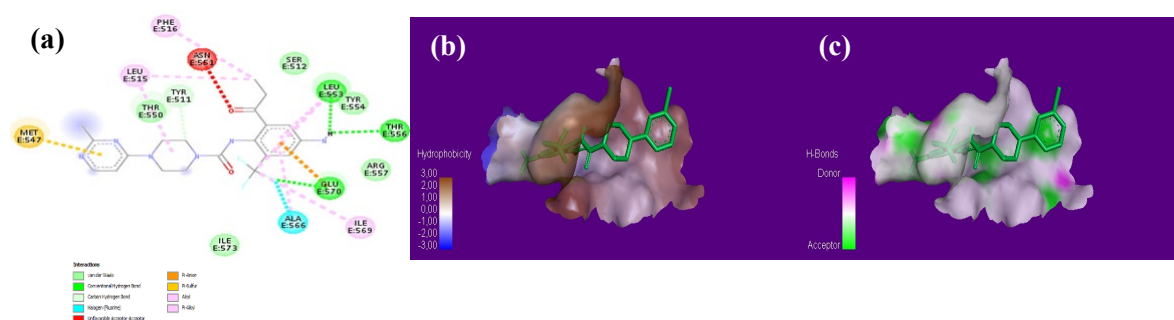


Fig. 10. Interaction of P2 with the protein (PDB ID: 5IS0). **(a)** 2D visualization of the interactions at the binding site; **(b)** hydrophobicity (3D view); and **(c)** 3D representation of the hydrogen bonding conformation.

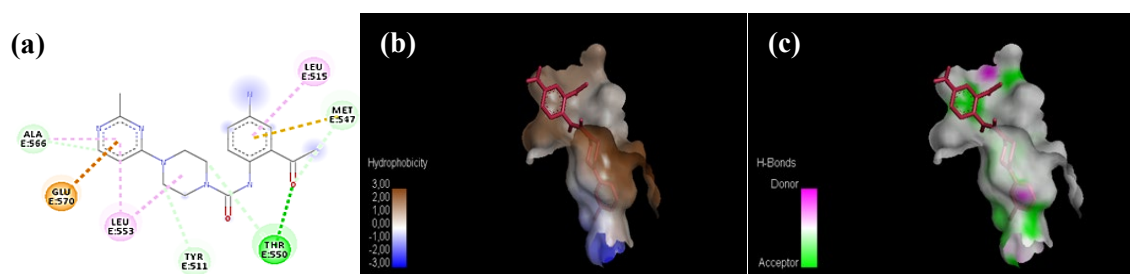


Fig. 11. Interaction of P3 with the protein (PDB ID: 5IS0). **(a)** 2D visualization of the interactions at the binding site; **(b)** hydrophobicity (3D view); and **(c)** 3D representation of the hydrogen bonding conformation.

The level of difference between the binding affinity values of the complexes is directly related to the stability of the protein-ligand interactions [35]. Figures 8, 9, 10 and 11 show the results of the interactions between the binding sites of compounds M07, P1, P2 and P3 and the receptor antagonist TRPV1 (PDB ID: 5IS0). Compound M07 established two hydrogen bonds with GLU C:570 and TYR C:511. two hydrophobic interactions with MET C:547 and GLU C:570. and three electrostatic interactions with LEU C:553, ILE C:569, and LEU C:515. The most active predicted compound P1 established four hydrogen bonds with LEU E: 553. THR E: 550. THR E: 556. and TYR E: 511. three

hydrophobic interactions with MET E: 547, ALA E: 566. and MET E: 547, as well as one electrostatic interaction with GLU E: 570. This type of interactions plays an important role in the stability of ligand-receptor complexes. In addition, hydrophobic and electrostatic interactions are generally associated with the affinity of ligand-protein bonds and their biological reactivity [34]. The predicted compounds P2 and P3 also established hydrogen bonds, electrostatic and hydrophobic interactions. The results are summarized in Table 6.

Table 6. Interactions of amino acids residues with ligands at receptor active site.

Ligands	Hydrogen-Binding Interaction	Hydrophobic Interaction	Electrostatic Interaction	Ligands	Hydrogen-Binding Interaction	Hydrophobic Interaction	Electrostatic Interaction
M07	GLUC:570 TYRC:511	MET C:547 GLUC:570	LEUC:553 ILE C:569 LEUC:515	P2	LEU E:553 THRE:556 GLUE:557 THR E:550	METE:573 GLUE:553	GLUC:570 LEUE:516 LEUE:553 ILE E:569
P1	THRE:550 LEUE:553 TYRE:511 THRE:556	LEUE:515 ALAE:566 METE:547	GLUE:570	P3	ALAE:557 METE:547 TYRE:511 THRE:550	GLUE:570 METE:547	LEUE:566 ALAE:515 LEUE:553

ADMET prediction

ADMET prediction is a very important method in drug design [36,37] because it helps identify pharmacokinetic properties, and toxicity properties of drug candidate of compound before wasting time and money on costly preclinical and clinical studies.

Before starting the experimental process, it is crucial to verify the pharmacokinetic properties [38,39] of the new compounds envisaged. Therefore, to carry out this step, ADMET (Absorption; Distribution; Metabolism; Excretion and Toxicity) prediction tests were performed using the pkCSM [40] and Swiss-ADMET [41] web servers. The results obtained were listed in Table 7.

According to the results presented in Table 7, all the predicted compounds have moderate ADMET parameters [42]. The high intestinal absorption values in humans (AHI > 40 %) indicate that the predicted compounds are able to penetrate the intestinal membrane to a moderate extent. Compounds P1, P2 and P3 showed high values of Caco-2 permeability. None of the molecules were toxic [43] and also were not expected to inhibit the enzymes CYP2C19, CYP2D6, and CYP3A4. The synthetic accessibility of all the compounds was less than 10 and close to 1, which shows that their organic synthesis is relatively easy.

Conclusions

This study aims to present the development of new TRPV1 antagonist compounds obtained by 3D-QSAR studies using the CoMFA and CoMSIA methods. The results show high Q^2 , R^2 and R^2 test values for the performing models, and the molecular docking analysis shows synergy with the 3D-QSAR studies. Three new compounds (P1-3) were predicted with the CoMSIA method which showed high stability in the protein-binding pocket and possessed antagonistic potency more than of the most active molecule. The ADMET prediction indicates that the synthesis of these compounds is very accessible.

Acknowledgements

We dedicated this work to the “Moroccan Association of Chemists Theorists” (MACT) for its pertinent help concerning the programs.

Table 7. ADMET analysis and synthetic accessibility of predicted compounds.

Compounds	Absorption			Distribution	Metabolism							Excretion	Toxicity		Synthetic accessibility
	Water solubility	Caco2 permeability	Intestinal absorption human (HIA)	Blood Brain Barrier Permeability	CYP							Total Clearance	AMES toxicity	Max. tolerated dose (human)	
					2D6	3A4	1A2	2C19	2C9	2D6	3A4				
					Substrate		Inhibitor								
	Numeric (Log mol/L)	Numeric (log Papp in 10-6 cm/s)	Numeric (% Absorbed)	Numeric (log BB)	Categorical (Yes/No)							Numeric (log ml/min/kg)	Categorical (Yes/No)	Numeric (log mg/kg/day)	
P1	-2.653	-0.487	43.049	-1.811	NO	NO	NO	NO	NO	NO	NO	-0.075	NO	0.95	3.20
P2	-3.918	0.752	81.722	-1.623	NO	NO	NO	NO	YES	NO	YES	0.119	NO	0.136	3.22
P3	-3.485	0.845	78.661	-1.289	NO	NO	NO	NO	NO	NO	NO	-0.091	NO	0.025	2.80
M07	-3.963	1.328	92.638	-0.785	NO	NO	NO	NO	NO	NO	NO	0.098	NO	0.321	2.61

References

1. Smit, T.; Mayorga, N. A.; Rogers, A. H.; Nizio, P.; Zvolensky, M. J. *Addict. Behav.* **2023**, 136, 107495. DOI: <https://doi.org/10.1016/j.addbeh.2022.107495>
2. Schrepf, A.; Gallop, R.; Naliboff, B.; Harte, S. E.; Afari, N.; Lai, H. H.; Pontari, M.; McKernan, L. C.; Strachan, E.; Kreder, K. J.; et al. *J. Pain* **2022**, 23, 1594–1603. DOI: <https://doi.org/10.1016/j.jpain.2022.03.240>
3. Reilly, R. M.; McDonald, H. A.; Puttfarcken, P. S.; Joshi, S. K.; Lewis, L. G.; Pai, M.; Franklin, P. H.; Segreti, J. A.; Neelands, T. R.; Han, P.; et al. *J. Pharmacol. Exp. Ther.* **2012**, 342, 416–428. DOI: <https://doi.org/10.1124/jpet.111.190314>
4. Aghazadeh Tabrizi, M.; Baraldi, P. G.; Baraldi, S.; Gessi, S.; Merighi, S.; Borea, P. A. *Med. Res. Rev.* **2017**, 37, 936–983. DOI: <https://doi.org/10.1002/med.21427>
5. Toughzaoui, A.; Chedadi, O.; El Aissouq, A.; El Ouardi, Y.; Bouachrine, M.; Ouammou, A. *Phys. Chem. Res.* **2022**, 11, 353–368. DOI: <https://doi.org/10.22036/pcr.2022.334832.2059>
6. Csekő, K.; Beckers, B.; Keszthelyi, D.; Helyes, Z. *Pharmaceuticals*. **2019**, 12, 48. DOI: <https://doi.org/10.3390/ph12020048>
7. Seeböhm, G.; Schreiber, J. A. *Cell. Physiol. Biochem.* **2021**, 22, 108–130. DOI: <https://doi.org/10.33594/000000358>
8. Loyd, D. R.; Chen, P. B.; Hargreaves, K. M. *Neuroscience*. **2012**, 203, 207–215. DOI: <https://doi.org/10.1016/j.neuroscience.2011.12.019>
9. Sawhney, J. P.; Kothiwale, V. A.; Bisne, V.; Durgaprasad, R.; Jadhav, P.; Chopda, M.; Vanajakshamma, V.; Meena, R.; Vijayaraghavan, G.; Chawla, K.; et al. *Indian Heart J.* **2018**, 70. DOI: <https://doi.org/10.1016/j.ihj.2018.09.001>
10. Helyes, Z.; Csekő, K.; Beckers, B.; Keszthelyi, D. *Front. Pharmacol.* **2017**, 8, 121. DOI: <https://doi.org/10.3389/fphar.2017.00121>
11. Li, J.; Nie, C.; Qiao, Y.; Hu, J.; Li, Q.; Wang, Q.; Pu, X.; Yan, L.; Qian, H. *Eur. J. Med. Chem.* **2019**, 178, 433–445. DOI: <https://doi.org/10.1016/j.ejmech.2019.06.007>
12. Othman, A. A.; Nothaft, W.; Awni, W. M.; Dutta, S. *Br. J. Clin. Pharmacol.* **2013**, 75, 203–212. DOI: <https://doi.org/10.1111/j.1365-2125.2012.04405.x>
13. Benko, R.; Illényi, L.; Kelemen, D.; Papp, R.; Papp, A.; Bartho, L. *Eur. J. Pharmacol.* **2012**, 674, 44–50. DOI: <https://doi.org/10.1016/j.ejphar.2011.10.021>
14. Abdelgawad, M. A.; Elkanzi, N. A. A.; Musa, A.; Ghoneim, M. M.; Ahmad, W.; Elmowafy, M.; Abdelhaleem Ali, A. M.; Abdelazeem, A. H.; Bukhari, S. N. A.; El-Sherbiny, M.; et al. *Arab. J. Chem.* **2022**, 15, 104015 DOI: <https://doi.org/10.1016/j.arabjc.2022.104015>
15. Khurana, L.; Fu, B.; Duddupudi, A. L.; Liao, H.; Immadi, S. S.; Kendall, D. A.; Lu, D. *J. Med. Chem.* **2017**. DOI: <https://doi.org/10.1021/acs.jmedchem.6b01448>
16. Burkert, U.; Allinger, N. L., in: *Molecular Mechanics*; American Chemical Society: Washington, DC, **1982**.
17. Sousa, S. F.; Ribeiro, A. J. M.; Coimbra, J. T. S.; Neves, R. P. P.; Martins, S. A.; Moorthy, N. S. H. N.; Fernandes, P. A.; Ramos, M. J. *Curr. Med. Chem.* **2013**, 20, 2296–2314. DOI: <https://doi.org/10.2174/0929867311320180002>
18. Shamsad, H.; Hafiz, A.; Althagafi, I. I.; Saeed, M.; Mirza, A. Z. *Curr. Comput.-Aided Drug Des.* **2019**, 16. DOI: <https://doi.org/10.2174/1573409915666190827163327>
19. Nie, C.; Li, Q.; Qiao, Y.; Hu, J.; Gao, M.; Wang, Y.; Qiao, Z.; Wang, Q.; Yan, L.; Qian, H. *Eur. J. Med. Chem.* **2020**, 194, 112236. DOI: <https://doi.org/10.1016/j.ejmech.2020.112236>
20. Li, J.; Nie, C.; Qiao, Y.; Hu, J.; Li, Q.; Wang, Q.; Pu, X.; Yan, L.; Qian, H. *Eur. J. Med. Chem.* **2019**, 178, 433–445. DOI: <https://doi.org/10.1016/j.ejmech.2019.06.007>
21. Tong, L.; Guo, L.; Lv, X.; Li, Y. *J. Mol. Graphics Modell.* **2017**, 71, 1–12. DOI: <https://doi.org/10.1016/j.jmgm.2016.10.012>

22. Clark, M.; Cramer, R. D., III; Opdenbosch, N. V. *J. Comput. Chem.* **1989**, *10*, 982–1012. DOI: <https://doi.org/10.1002/jcc.540100804>
23. Chedadi, O.; El Aissouq, A.; El Ouardi, Y.; Bouachrine, M.; Ouammou, A. *Biointerface Res. Appl. Chem.* **2022**, *12*, 5100–5115. DOI: <https://doi.org/10.33263/BRIAC124.51005115>
24. El Aissouq, A.; Chedadi, O.; Bouachrine, M.; Ouammou, A. *J. Chem.* **2021**, 1901484. DOI: <https://doi.org/10.1155/2021/1901484>
25. El Aissouq, A.; El Hamdani, S.; El Mchichi, A.; Bouachrine, M. *Moroccan J. Chem.* **2022**, *10*. DOI: <https://doi.org/10.48317/IMIST.PRSM/morjchem-v10i4.34319>
26. Wang, A.; Yang, Y.; Jun, Y.; Wang, B.; Lv, K.; Liu, M.; Guo, H.; Lu, Y. *Bioorg. Med. Chem.* **2018**, *26*, 2073–2084. DOI: <https://doi.org/10.1016/j.bmc.2018.03.004>
27. Vrtačnik, M.; Voda, K. *Chemosphere* **2003**, *52*, 1689–1699. DOI: [https://doi.org/10.1016/S0045-6535\(03\)00354-0](https://doi.org/10.1016/S0045-6535(03)00354-0)
28. A. Chiari, L. P.; da Silva, A. P.; Honório, K. M.; da Silva, A. B. F. *J. Mol. Model.* **2023**, *29*, 1–3. DOI: <https://doi.org/10.1007/s00894-023-05443-5>
29. Ai, Y.; Wang, S. T.; Sun, P. H.; Song, F. J. *Int. J. Mol. Sci.* **2011**, *12*, 1605–1624. DOI: <https://doi.org/10.3390/ijms12031605>
30. Srivastava, P.; Tripathi, P. N.; Sharma, P.; Rai, S. N.; Singh, S. P.; Srivastava, R. K.; Shankar, S.; Shrivastava, S. K. *Eur. J. Med. Chem.* **2019**, *163*, 116–135. DOI: <https://doi.org/10.1016/j.ejmech.2018.11.049>
31. Dar, A. M.; Mir, S. J. *Anal. Bioanal. Tech.* **2017**, *8*, 8–10. DOI: <https://doi.org/10.4172/2155-9872.1000356>
32. El Bahi, S.; Boutalaka, M.; El Alaouy, M. A.; Bouamrane, S.; Alaqarbeh, M.; Choukrad, M.; Sbair, A.; Bouachrine, M.; Lakhliifi, T. *New J. Chem.* **2023**, *47*, 12816–12829. DOI: <https://doi.org/10.1039/D3NJ02471G>
33. Moukhliiss, Y.; Koubi, Y.; Alaqarbeh, M.; Rehman, H. M.; Maghat, H.; Sbair, A.; Bouachrine, M.; Lakhliifi, T. *ChemistrySelect* **2023**, *8*, e202203908. DOI: <https://doi.org/10.1002/slct.202203908>
34. Madhavilatha, N.; Rama, G.; Babu, M.; Afriza, D.; Suriyah, W. H.; Ichwan, S. J. A. *J. Phys.: Conf. Ser.* **2018**, *1073*, 032001. DOI: <https://doi.org/10.1088/1742-6596/1073/3/032001>
35. Varadharajan, A.; Sinha, S.; Xu, A.; Daniel, A.; Kim, K.; Shanmugam, N.; Wu, E.; Yang, C.; Zhang, M.; Acree, W. E. *J. Solution Chem.* **2023**, *52*, 70–90. DOI: <https://doi.org/10.1007/s10953-022-01215-6>
36. El Aissouq, A. E.; Chedadi, O.; Bouachrine, M.; Khalil, F. *J. Biomol. Struct. Dyn.* **2022**, *1*, 14. DOI: <https://doi.org/10.1080/07391102.2022.2071341>
37. Boutalaka, M.; El Bahi, S.; Alaqarbeh, M.; El Alaouy, M. A.; Koubi, Y.; Khatabi, K. E.; Maghat, H.; Bouachrine, M.; Lakhliifi, T. *J. Biomol. Struct. Dyn.* **2023**, 1–20. DOI: <https://doi.org/10.1080/07391102.2023.2233629>
38. Voight, E. A.; Gomtsyan, A. R.; Daanen, J. F.; Perner, R. J.; Schmidt, R. G.; Bayburt, E. K.; Didomenico, S.; McDonald, H. A.; Puttfarcken, P. S.; Chen, J.; et al. *J. Med. Chem.* **2014**, *57* (17), 7412–7424. DOI: <https://doi.org/10.1021/jm500916t>
39. Reda El-Mernissi Ayoub Khaldan, T. L.; Bouamrane, S.; Rehman, H. M.; Alaqarbeh, M.; Ajana, M. A.; Bouachrine, M. *J. Biomol. Struct. Dyn.* **2023**, 1–18. DOI: <https://doi.org/10.1080/07391102.2023.2214233>
40. Roth, H. S.; Botham, R. C.; Schmid, S. C.; Fan, T. M.; Dirikolu, L.; Hergenrother, P. J. *J. Med. Chem.* **2015**, *58*, 4046–4065. DOI: <https://doi.org/10.1021/acs.jmedchem.5b00413>
41. Daina, A.; Michielin, O.; Zoete, V. *Sci. Rep.* **2017**, *7*, 42717. DOI: <https://doi.org/10.1038/srep42717>
42. Abdessadak, O.; Alaqarbeh, M.; Zaki, H.; Almohtaseb, F.; Alsakhen, N.; Ajana, M. A.; Lakhliifi, T.; Bouachrine, M. *Struct. Chem.* **2023**, *34*, 1173–1187. DOI: <https://doi.org/10.1007/s11224-022-02068-x>